WATER RESOURCES RESEARCH, VOL. 34, NO. 12, PAGES 3315–3322, DECEMBER 1998

Mixing and stretching efficiency in steady and unsteady groundwater flows

Scott W. Weeks and Garrison Sposito

Department of Civil and Environmental Engineering, University of California, Berkeley

Abstract. Mixing is the physical process through which solute is spread into a fluid by the stretching and folding of material lines and surfaces. Mixing, as compared to dilution, is important to solute spreading by groundwater because it operates on much shorter timescales than does dilution, and it provides the increased plume boundary area and high local concentration gradients that promote effective solute dilution. In this paper, the mixing process is investigated theoretically for subsurface tracer plume movement, using as heuristic examples both steady and unsteady groundwater flows in a perfectly stratified aquifer whose properties mimic those of the sand aquifer at the Borden site. It is shown that the stretching efficiency, a parameter that characterizes the effectiveness of mixing, is largest at transitions between regions of highly contrasting hydraulic conductivity and, more broadly, that pronounced spatial variability in the hydraulic conductivity is conducive to good mixing because of the periodic resurgences in material line stretching that it causes. Unsteady groundwater flow resulting from a decrease in vertical groundwater flux with time leads to greater rates of material line stretching than do steady flows, whereas little difference from the steady flow case occurs for unsteady groundwater flow under a time-varying horizontal hydraulic head gradient. Overall, pronounced spatial variability in the hydraulic conductivity is the most important contributor to good mixing of a tracer solute plume, but highly effective mixing requires additional physical conditions that induce chaotic solute pathlines.

1. Introduction

Solute plumes moving in aquifers are spread by two important but quite distinct physical processes. One is termed dilution, through which a plume is gradually distributed over an ever increasing volume of an aquifer to produce a reduction in solute concentration. Dilution is driven by local dispersion (i.e., dispersion processes occurring at the Darcy scale) and, secondarily, by complexity in plume shape, which serves to increase the plume boundary area through which solute mass can be transported dispersively. *Kitanidis* [1994] has defined a "dilution index" to quantify the effectiveness of this physical process. The dilution index always increases as a solute plume acted upon by local dispersion becomes more dilute, but it remains constant if local dispersion is insignificant, regardless of how a plume may be evolving with time [*Kitanidis*, 1994]. *Thierrin and Kitanidis* [1994] and *Kapoor and Kitanidis* [1998a, b] have discussed applications of the dilution index to tracer plume spreading by groundwater as observed in field experiments and in computer simulations of flow in model porous media.

In contrast to dilution, mixing is the process through which solute is spread into a fluid by the stretching and folding of material lines and surfaces [*Ottino*, 1989, section 1.4; 1990, p. 209]. Mixing is thus driven by advection (especially unsteady advection) which acts to stretch and fold fluid filaments in such a manner that plume boundary areas become highly irregular in shape and enlarged, while concentration gradients normal to the stretched filaments are increased greatly. Mixing has long been recognized as a key physical process affecting the spreading of a solute plume by turbulent fluid motions [*Batchelor*, 1952; *Moffatt*, 1983]. A principal effect of mixing in this case is a reduction in the length scales over which concentration gradients occur as material volume elements are thinned [*Batchelor*, 1952; *Ottino*, 1991]. In groundwater flow a pronounced spatial variability of the hydraulic conductivity will produce a specific discharge field that in some ways can be likened to a turbulent fluid velocity field, and the early phase of spreading of a solute plume into pristine groundwater should similarly be governed not by dilution but instead by advective stretching and folding of material lines and surfaces. This early behavior appears clearly in the tracer plume simulation reported by *Kapoor and Kitanidis* [1998a, Figure 4a], who found that the dilution index actually decreases concurrently with severe advective distortion of a solute concentration field.

Mixing processes in groundwater have not been investigated systematically, although their existence was noted in passing by *Kitanidis* [1994] and *Kapoor and Kitanidis* [1998a]. However, mixing phenomena, being important much earlier in the spreading of a solute plume than is dilution, create the complex plume-groundwater interface that enhances local dispersion processes [*Ottino*, 1991; *Kitanidis*, 1994; *Kapoor and Kitanidis*, 1998a]. In this paper we discuss basic concepts of plume mixing into groundwater, following the conceptual design of *Ottino* [1989, chapters 2 and 4; 1990], who considered fluid flows that were engineered to enhance mixing. The ideas we present are illustrated by tracer plume mixing during both steady and unsteady groundwater flows in a perfectly stratified aquifer, a model system whose tractability permits facile exposure of the main physical and mathematical issues. The mixing characteristics of unsteady groundwater flows are developed

Copyright 1998 by the American Geophysical Union.

Paper number 98WR02535.
0043-1397/98/98WR-02535$09.00

and compared to those of the steady flow case. Unsteady flow is introduced in two steps. First, the magnitude of the horizontal hydraulic head gradient is allowed to vary with time, then the vertical coordinate of the specific discharge vector is converted to a time-varying parameter. Neither case violates the simplifying condition of a solenoidal specific discharge field. By allowing the flow to become unsteady in steps, we expect to see more clearly how time-dependent aspects of groundwater movement can improve solute mixing.

2. Quantification of Mixing

By definition, the mixing of a tracer plume into groundwater involves the stretching of material lines. If **M** is a unit vector tangent to a material line element in some state of a fluid that has been selected as a reference against which to evaluate stretching, and if $\bar{F}$ is the deformation gradient tensor [*Eringen*, 1980, section 1.4] that relates a line element in some present state of the fluid to its counterpart in the reference state, then the length stretch λ caused by fluid deformation is defined by the equation [*Ottino*, 1989, section 2.6]

$$\lambda \mathbf{m} = \bar{F} \cdot \mathbf{M} \tag{1}$$

where **m** is a unit vector tangent to the material line element in the deformed fluid state. Because **M** is a constant vector by definition, the time dependence of the left side of (1) derives entirely from that of the tensor $\bar{F}$. (A full introductory discussion of the physical significance of $\bar{F}$ is given, e.g., by *Eringen* [1980, chapter 1].) The resulting expression for the material derivative of λ is [*Ottino*, 1989, section 2.9]:

$$D\lambda/Dt = (\mathbf{m} \cdot \bar{\mathbf{D}} \cdot \mathbf{m})\lambda \tag{2}$$

where

$$\bar{\mathbf{D}} = \tfrac{1}{2}[\nabla \mathbf{v} + (\nabla \mathbf{v})^T] \tag{3}$$

is the "fluid stretching tensor," i.e., the symmetric part of the fluid velocity gradient $\nabla \mathbf{v}$ [*Eringen*, 1980, section 2.6]. Equations (2) and (3) show that time dependence in λ occurs whenever the component of the fluid velocity gradient along the unit vector **m** does not vanish. Physically, this nonvanishing component implies that variations in fluid velocity along a material line element, (i.e., $\mathbf{m} \cdot \nabla \mathbf{v}$) are acting to stretch (or contract) the line element [*Batchelor*, 1992, section 5.2].

The unit eigenvectors of the symmetric tensor $\bar{\mathbf{D}}$ in (3) prescribe the directions along which fluid stretching takes on extremum values [*Ottino*, 1989, section 2.11, appendix]. Thus the tensor element $\mathbf{m} \cdot \bar{\mathbf{D}} \cdot \mathbf{m}$ is an extremum if **m** is a unit eigenvector of $\bar{\mathbf{D}}$. Application of the Cauchy-Schwartz inequality to this tensor element shows that [*Ottino*, 1989, section 4.1]

$$|\mathbf{m} \cdot \bar{\mathbf{D}} \cdot \mathbf{m}|^2 \leq |\bar{\mathbf{D}}|^2 \tag{4}$$

since **m** is a unit vector, where, in terms of the fluid stretching tensor elements $\bar{D}_{ij}$,

$$|\bar{\mathbf{D}}|^2 \equiv \sum_i \sum_j \bar{D}_{ij}\bar{D}_{ji} \tag{5}$$

is the square of the scalar magnitude of $\bar{\mathbf{D}}$, denoted $|\bar{\mathbf{D}}|$. The magnitude of a symmetric tensor can be evaluated in any convenient set of basis vectors, including that of its eigenvectors, which fact also shows that the right side of (5) is always equal numerically to the sum of the squares of the eigenvalues of $\bar{\mathbf{D}}$ [*Ottino*, 1989, appendix].

Given (4), it is reasonable to define the stretching efficiency of the line element whose unit tangent vector is **m** by the equation [*Ottino*, 1989, section 4.1]

$$e_\lambda \equiv \frac{|D \ln \lambda/Dt|}{|\bar{\mathbf{D}}|} = \frac{|\mathbf{m} \cdot \bar{\mathbf{D}} \cdot \mathbf{m}|}{|\bar{\mathbf{D}}|} \tag{6}$$

Clearly, e_λ lies between 0 and 1, thus providing an objective (i.e., frame indifferent) measure of how well a given material line element is stretched (or contracted) by a fluid velocity field.

Ottino [1989, chapter 4] presents a number of calculations of e_λ and ln λ for fluid motions that are relevant to engineered mixing systems. He notes that for isochoric fluid flows (i.e., solenoidal velocity fields), the maximum value of e_λ in three dimensions is $(2/3)^{-1/2} \approx 0.816$, whereas in two dimensions it is $2^{-1/2} \approx 0.707$. This latter result follows directly from the constraint,

$$\sum_{i=1}^{2} D_{ii} = \nabla \cdot \mathbf{v} = \delta_1 + \delta_2 = 0 \tag{7}$$

which applies to any two-dimensional, solenoidal velocity field, where δ_1 and δ_2 are the two equal and opposite eigenvalues of $\bar{\mathbf{D}}$ [*Ottino*, 1989, appendix]. Since a maximum in $|\mathbf{m} \cdot \bar{\mathbf{D}} \cdot \mathbf{m}|$, and therefore in e_λ, occurs when **m** is a unit eigenvector of $\bar{\mathbf{D}}$, it follows from (6) and (7) that the maximum stretching efficiency is

$$e_\lambda(\max) = \frac{\delta_1}{|\bar{\mathbf{D}}|} = \frac{\delta_1}{(\delta_1^2 + \delta_2^2)^{1/2}} = \frac{\delta_1}{(2\delta_1^2)^{1/2}} = 2^{-1/2} \tag{8}$$

where δ_1 is selected as the positive eigenvalue of $\bar{\mathbf{D}}$.

A fundamental physical quantity related to (2) is the time average of the relative length-stretching rate [*Ottino*, 1990]:

$$\frac{1}{T}\int_0^T \frac{D}{Dt} \ln \lambda \, dt = \frac{1}{T} \ln [\lambda(T)/\lambda(0)] \qquad T > 0 \tag{9}$$

Good mixing is defined to occur whenever the right side of (9) is positive and independent of the orientation of **M** [*Ottino*, 1990, 1991], because material line elements in a plume boundary then are growing exponentially with time over the interval $0 < t < T$. Exponential growth of material line elements over very long time intervals is one of the signatures of fluid path line chaos [*Ottino*, 1989, section 5.8.2; 1990, p. 219]. This type of fluid motion is quantified by the infinite-time limit of (9),

$$\sigma \equiv \lim_{T \uparrow \infty} \frac{1}{T} \ln [\lambda(T)/\lambda(0)] \tag{10}$$

which is termed the Liapunov exponent associated with stretching of the material line element to which λ refers. A sufficient requirement for chaotic behavior of the pathlines generated by a fluid velocity field is that σ have a positive value [*Ottino*, 1990], which amounts to a nonzero asymptotic (large time) average value for the relative rate of line stretching in (2). This condition of "Lagrangian chaos" portends severe solute plume distortion and therefore highly effective mixing [*Ottino*, 1990, 1991].

3. Groundwater Flow in a Perfectly Stratified Aquifer: Illustrative Cases

Sposito and Weeks [1998] have demonstrated that steady flows of groundwater described by the model specific discharge expression,

$$\mathbf{q}(z) = K(z)J_x\hat{x} + K(z)J_y\hat{y} + q_z\hat{z} \tag{11}$$

where circumflexes denote unit vectors along Cartesian axes, are confined to a family of nonintersecting permanent surfaces on which lie both the stream lines of $\mathbf{q}(z)$ and the field lines of its vorticity vector,

$$\mathbf{w}(z) = \nabla \times \mathbf{q} = \frac{dK}{dz}(-J_y\hat{x} + J_x\hat{y}) \tag{12}$$

Equation (11) represents a solenoidal specific discharge field ($\nabla \cdot \mathbf{q} = 0$) in a perfectly stratified aquifer whose strata are congruent with the $x - y$ plane. The horizontal components of the hydraulic head gradient, $-J_x$ and $-J_y$, are uniform, whereas along the direction perpendicular to the strata, the specific discharge coordinate q_z is uniform because $\mathbf{q}$ is solenoidal. *Sposito and Weeks* [1998] illustrated the topology of steady flows governed by (11) using data for $K(z)$, J_x, J_y, and q_z that were applicable to the sand aquifer at the Borden site in Ontario, Canada [*Roberts and Mackay*, 1986; *Freyberg*, 1986; *Turcke and Kueper*, 1996].

A simple generalization of (11) results from permitting the horizontal head gradient and the vertical specific discharge to become explicitly time dependent:

$$\mathbf{q}(z, t) = K(z)J_x(t)\hat{x} + K(z)J_y(t)\hat{y} + q_z(t)\hat{z} \tag{13}$$

where

$$J_x(t) = J(t) \sin \varphi \tag{14a}$$

$$J_y(t) = J(t) \cos \varphi \tag{14b}$$

The angle $\varphi \equiv \tan^{-1}[J_x(t)/J_y(t)]$ defines the constant direction of the horizontal head gradient in the $x - y$ plane, $J(t)$ being its time-dependent magnitude, where $J(t) \equiv [J_x^2(t) + J_y^2(t)]^{1/2}$. Permitting φ to be time dependent is an additional possibility for creating unsteady flow, but this would only rotate the pathlines of $\mathbf{q}(z, t)$ without stretching them. It will prove useful to exploit the symmetry inherent in (13) and (14) to transform (13) into a cylindrical polar coordinate system (ρ, φ, z):

$$\mathbf{q}(z, t) = K(z)J(t)\hat{\rho} + q_z(t)\hat{z} \tag{15}$$

Equation (15) describes a solenoidal specific discharge vector that is confined to the $\rho - z$ plane, with the fixed polar angle φ defining the direction of the ρ axis relative to the Cartesian y axis.

The path lines of spatial points ("fluid particles") moving in unsteady flow under (13) are solutions of the ordinary differential equation [*Eringen*, 1980, section 2.3; *Ottino*, 1989, section 2.4]:

$$\frac{d\mathbf{c}}{ds} = \frac{\mathbf{q}(z, t)}{q(z, t)} \tag{16}$$

where $q(z, t) = \{[K(z)J(t)]^2 + [q_z(t)]^2\}^{1/2}$ and s is arc length as measured along a path line; i.e., $ds/dt = q(z, t)/n$, n being the aquifer porosity. Thus

$$x(t) = \frac{1}{n}\int_0^t K[z(t')]J_x(t')\,dt' \tag{17a}$$

$$y(t) = \frac{1}{n}\int_0^t K[z(t')]J_y(t')\,dt' \tag{17b}$$

$$z(t) = \frac{1}{n}\int_0^t q_z(t')\,dt' \tag{18}$$

is a solution of (16) in terms of Cartesian coordinates parameterized by time. The corresponding path lines, as they would appear in the $\rho - z$ plane, are shown in Figure 1 along with those for steady flow under (15). To construct them, permeability data from *Turcke and Kueper* [1996] (second core along the transect in their Figure 2) were converted to the $K(z)$ profile in Figure 2 using conventional cubic spline interpolation [*Press et al.*, 1992]. The overall characteristics of this conductivity profile include a harmonic mean, $K_H = 2.73$ m d^{-1}, and an arithmetic mean, $K_A = 7.76$ m d^{-1}, the latter being close to the Borden aquifer-wide hydraulic conductivity value, ~8 m d^{-1}, cited by *Thierrin and Kitanidis* [1994] and *Turcke and Kueper* [1996]. The value of φ in (14) has been taken as 11° east of north, approximately the mean direction of progress of the center of mass of a tracer plume at the Borden site as reported by *Farrell et al*. [1994, Figure 10]. The data for $J(t)$ shown in Figure 3 were also obtained from *Farrell et al*. [1994, Figure 7b] and smoothed by cubic spline interpolation. The aquifer porosity n is equal to 0.33, the mean value at the Borden site [*Thierrin and Kitanidis*, 1994].

The two unsteady flow cases share a common $J(t)$, but case B has a constant q_z, whereas case C has a q_z that varies with time. In Figure 1, $q_z = 2.76405$ mm d^{-1}, a constant value calculated by *Sposito and Weeks* [1998] in order to have $\rho(z) = 20$ m when $z = 2$ m under steady flow [*Freyberg*, 1986, Figure 7a], and $q_z(t) = n\, dz_f/dt$, where $z_f(t)$ also comes from *Freyberg* [1986, Figure 7b], who presented the displacement, in the $\rho - z$ plane, of the center of mass of a tracer plume at the Borden site. The resultant $q_z(t)$ profile is shown in Figure 4 compared with its 2-year mean value (1.23841 mm d^{-1}) and the constant value $q_z = 2.76405$ mm d^{-1}. The peak values of $q_z(t)$ during the early phase of motion in Figure 4 account for the earlier and more rapid vertical drop of the path line for case C compared to those for cases A and B.

4. Stretching Efficiency

For the specific discharge vector in (15),

$$\nabla\mathbf{v} = \frac{dK}{dz}\frac{J(t)}{n}\hat{z}\hat{\rho} \tag{19}$$

in a dyadic representation, such that the "fluid stretching tensor" for the specific discharge field has the corresponding dyadic form:

$$\bar{\mathbf{D}} = \frac{1}{2}\frac{dK}{dz}\frac{J(t)}{n}(\hat{z}\hat{\rho} + \hat{\rho}\hat{z}) \tag{20}$$

The coefficient of the unit-dyadic terms in (20) is proportional to the magnitude of the vorticity based on (15):

$$\mathbf{w}(z, t) = \nabla \times q(z, t) = \hat{z} \times dq/dz = dK/dzJ\hat{\varphi} \tag{21}$$

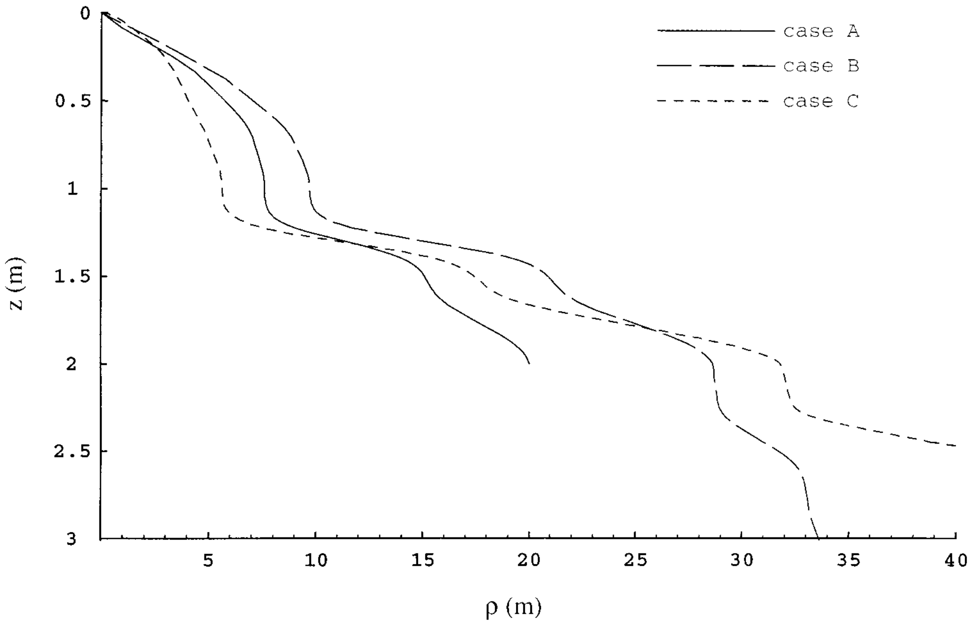

Figure 1. Pathlines for the three groundwater flow cases listed in Table 1.

which, like $\mathbf{w}(z, t)$ in (12), always lies in a stratum of the aquifer, perpendicular to a pathline in the $\rho - z$ plane. It follows from (5) and (20) that

$$|\bar{\mathbf{D}}| = \frac{1}{\sqrt{2}} \frac{dK}{dz} \frac{J(t)}{n} \tag{22}$$

The eigenvalues of $\bar{\mathbf{D}}$ can be calculated by conventional algebraic methods, to yield [*Ottino*, 1989, appendix]

$$\delta_1 = \frac{1}{\sqrt{2}} |\bar{\mathbf{D}}|, \qquad \delta_2 = 0, \qquad \delta_2 = \frac{-1}{\sqrt{2}} |\bar{\mathbf{D}}| \tag{23}$$

the second of which corresponds to the absence of stretching along the $\hat{\varphi}$ direction (i.e., $\bar{\mathbf{D}} \cdot \hat{\varphi} = \mathbf{O}$).

The length stretch λ of a material line element then satisfies (2) in the form

$$\frac{D}{Dt} \ln \lambda = \frac{dK}{dz} \frac{J(t)}{n} (\mathbf{m} \cdot \hat{z})(\mathbf{m} \cdot \hat{\rho}) = \frac{dK}{dz} \frac{J(t)}{n} \cos \theta \sin \theta$$

$$= \frac{1}{2} \frac{dK}{dz} \frac{J(t)}{n} \sin 2\theta \tag{24}$$

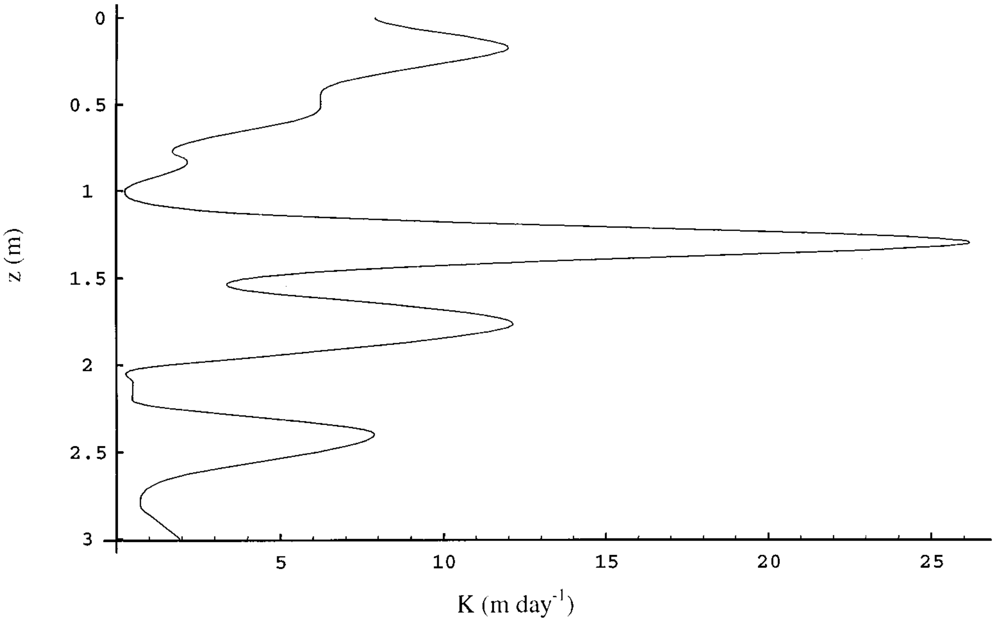

Figure 2. The hydraulic conductivity profile (Borden site) used in constructing the path lines in Figure 1 [*Turcke and Kueper*, 1996; *Sposito and Weeks*, 1998].

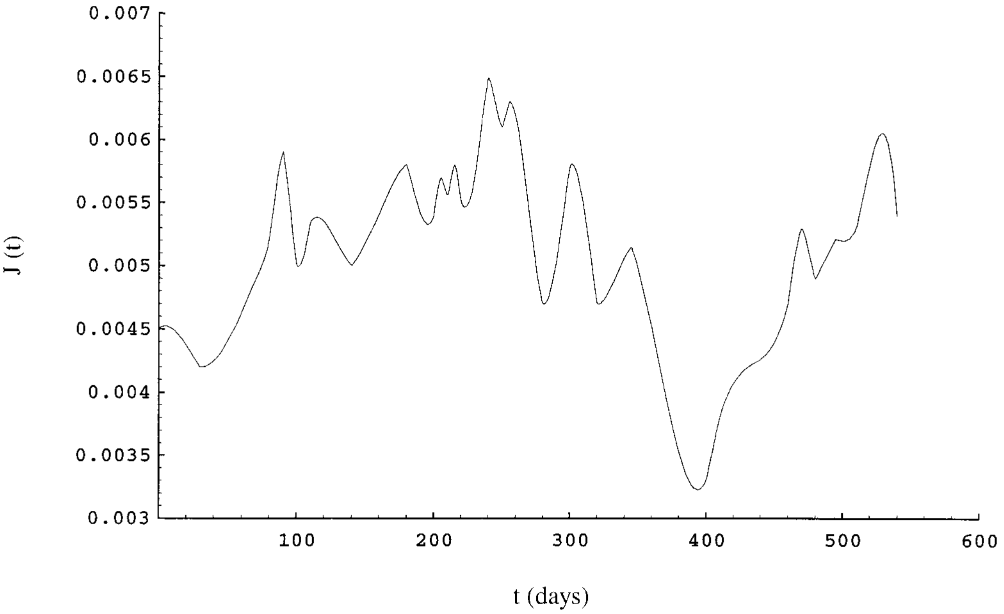

Figure 3. The magnitude of the time-dependent hydraulic head gradient $J(t)$ at the Borden site (redrawn from *Farrell et al.* [1994, Figure 7(a)] with permission from Elsevier Science).

where θ is the azimuthal angle between $\mathbf{m}$ and the z axis (i.e., $\mathbf{m} \cdot \hat{z} \equiv \cos\theta$). The corresponding stretching efficiency then follows from (6), (22), and (24):

$$e_\lambda = \frac{1}{\sqrt{2}} \sin 2\theta \tag{25}$$

Equation (25) shows that when $\theta = \pi/4$ (45°), the stretching efficiency achieves the largest value possible for isochoric, two-dimensional fluid flow, e_λ (max) $= 1/\sqrt{2}$, as derived in (8). This condition is met in the present case wherever the unit vector $\mathbf{m}$ makes equal angles with the ρ and z axes.

A specific example is afforded by taking $\mathbf{m} = d\mathbf{c}/ds$ in (16):

$$\mathbf{m} \equiv \sin\theta\hat{\rho} + \cos\theta\hat{z} = \frac{K(z)J(t)}{q(z,t)}\hat{\rho} + \frac{q_z(t)}{q(z,t)}\hat{z} \tag{26}$$

The resulting form of (24) for the relative rate of length stretching is then

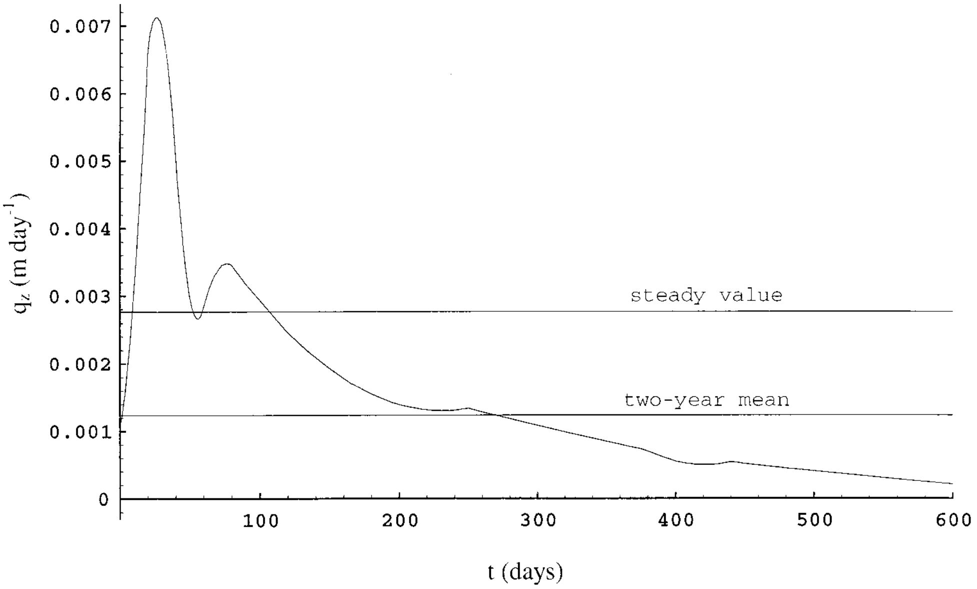

Figure 4. The temporal profile of $q_z(t)$ used in constructing the path line in Figure 1 for case C (Table 1), where $q_z(t) = n\, dz_f/dt$ and porosity $n = 0.33$ [*Thierrin and Kitanidis*, 1994], with $z_f(t)$ from *Freyberg* [1986, Figure 7b]. The 2-year mean value of $q_z(t)$ is 1.23841 mm d^{-1}, indicated by the lower horizontal line, while the upper horizontal line indicates the constant value $q_z = 2.76405$ mm d^{-1}, appropriate to cases A and B (Table 1).

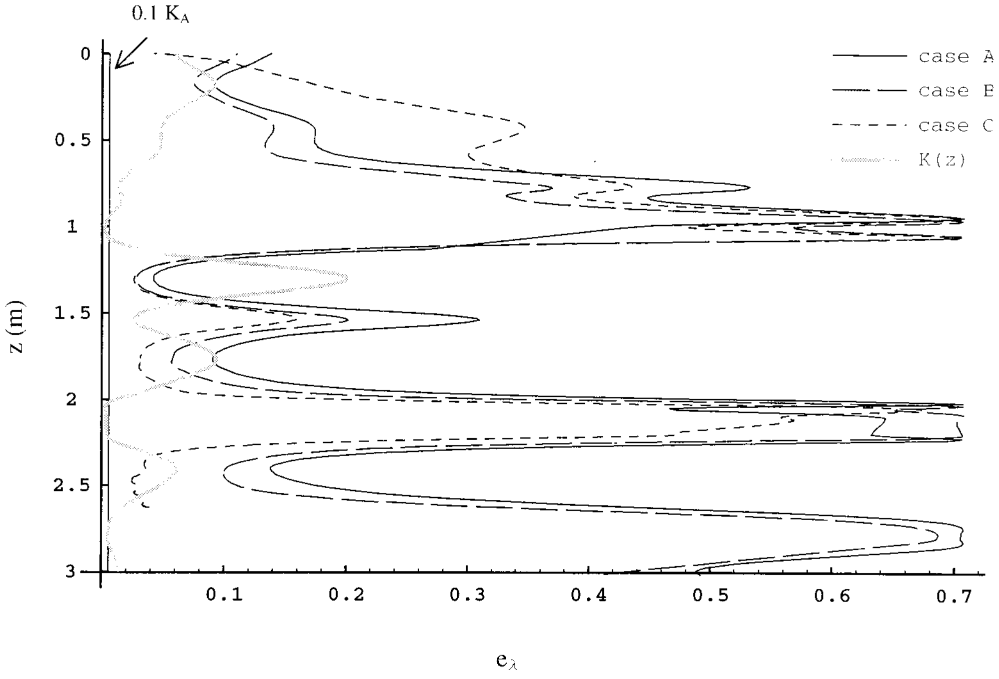

Figure 5. Vertical profile of the stretching efficiency e_λ, following a path line through a transect of the aquifer at the Borden site for the three flow cases listed in Table 1. The $K(z)$ profile shown has been scaled by $0.2/K_{\max}$. *Sudicky* [1986] finds that q_z (the value used for case A) is 10% of the mean horizontal coordinate of the specific discharge, i.e., $q_z = 0.1\ K_A J$. The vertical line at left represents the value of $0.1\ K_A = 0.776$ m d^{-1} (also scaled by $0.2/K_{\max}$). Note that maximum stretching occurs for case A wherever the $K(z)$ profile crosses this line (i.e., whenever $K = 0.1\ K_A = q_z/J$).

$$\frac{D}{Dt}\ln\lambda = \frac{dK}{dz}\frac{J(t)}{n}\left(\frac{q_z(t)}{q(z,t)}\right)\left(\frac{K(z)J(t)}{q(z,t)}\right) = \frac{q_z(t)}{nq(z,t)}\left(\frac{\partial q}{\partial z}\right)_t$$

$$= \frac{q_z(t)}{n}\left(\frac{\partial}{\partial z}\ln q\right)_t \qquad (27)$$

which shows that the relative stretching rate is enhanced significantly where $q(z, t)$ is changing most rapidly along the vertical direction in the aquifer. The stretching efficiency corresponding to (27) is

$$e_\lambda = \frac{\sqrt{2}K(z)J(t)q_z(t)}{[q(z,t)]^2} \qquad (28)$$

which reaches its maximum value whenever $K(z)J(t) = q_z(t)$, according to the definition of the angle θ in (26).

Figure 5 presents e_λ as a function of depth following a path line in the aquifer, based on (18), (28), and the relevant data for the three cases summarized in Table 1. Comparison of Figures 2 and 5 indicates that the stretching efficiency achieves its maximum theoretical value ($\approx$0.71) as a pathline traverses between minimum and maximum values of the hydraulic conductivity (gray line curve superimposed in Figure 5). The effects of time dependence in the horizontal hydraulic head gradient and in the vertical coordinate of specific discharge are more evident in Figure 6, which shows e_λ as a function of time, again following a path line, using (18), (28), and relevant data for the three cases summarized in Table 1. The consequence of a time-varying horizontal hydraulic head gradient, $J(t)$ in Figure 3, is relatively small, producing a temporal stretching efficiency profile (case B) that is almost coincident with that obtained for constant J (case A). By contrast, the temporal profile of e_λ that results from a time-varying vertical specific discharge, $q_z(t)$ in Figure 4, is both shifted (at $t < 200$ days) and broadened (for $t \approx 300$ days) relative to the profile obtained for constant q_z (case A or B). The time shift can be attributed to the larger values of $q_z(t)$, relative to q_z, when $t < 100$ days (Figure 4), whereas broadening occurs because of the pronounced decline in $q_z(t)$ for $t > 250$ days, which causes a moving spatial point to linger while traversing the peak in $K(z)$ just above $z \approx 2$ m (Figure 2).

Table 1. Groundwater Flow Parameters for Three Cases Illustrating Fluid Stretching

Flow Case	$K(z)$	$J(t)$	$q_z(t)$
A (steady)	Figure 2	0.00356	2.76405 mm d^{-1}
B (unsteady)	Figure 2	Figure 3	2.76405 mm d^{-1}
C (unsteady)	Figure 2	Figure 3	Figure 4

Data for $K(z)$ from *Turcke and Kueper* [1996]. Data for constant J from *Roberts and Mackay* [1986]. Data for time-varying J from *Farrell et al.* [1994]. Data for $q_z(t)$ from *Freyberg* [1986].

Equation (27) can be solved readily after substitution of the right side of (18) for the variable z, thus converting the Eulerian material derivative of λ to a Lagrangian partial derivative with respect to time at a fixed initial value of $z(t)$. The solution of (27) is then:

$$\ln\lambda[z(t), t] = \ln q[z(t), t] - \int_0^t \left(\frac{\partial \ln q}{\partial \tau}\right)_{z(\tau)} d\tau + c_1 \qquad (29)$$

where $z(t)$ is given by (18) with $z(0) = 0$, and the constant of integration c_1 is determined by the choice of reference state

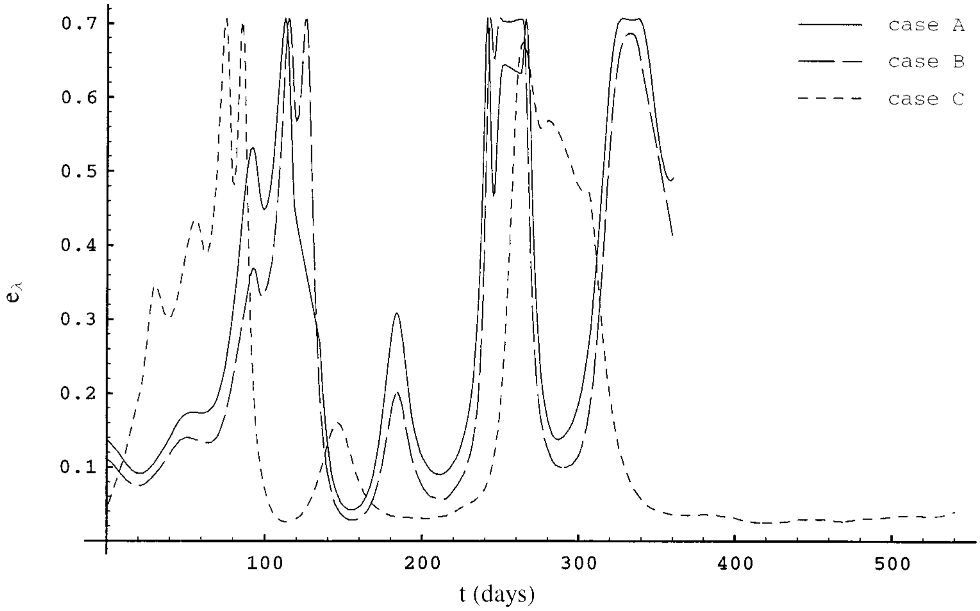

Figure 6. The stretching efficiency e_λ as a function of time, again following a path line, for the three flow cases listed in Table 1.

for which $\lambda = 1$. Figure 7 shows temporal profiles of ln $\lambda[z(t), t]$ for cases A and C in Table 1, based on a reference state at $z = 1$ m, where $K(z)$ has its smallest value (Figure 2). For this choice of reference state, $\lambda > 1$ at all times during steady flow (case A). During unsteady flow (case C), however, $\lambda < 1$ between 260 and 310 days because the length stretch is no longer controlled solely by the magnitude of the specific discharge vector (i.e., path lines are no longer congruent with streamlines). Indeed, under steady flow (case A), the oscillatory behavior of ln λ simply mirrors that of $K(z)$ in Figure 2, demonstrating the effectiveness of a spatially varying hydraulic conductivity in producing stretching. By contrast, the oscillations in ln λ under unsteady flow (case C) are time shifted ($t <$ 200 days), broadened ($t >$ 150 days), and intensified ($t <$ 100 days) relative to those in ln λ under steady flow (case A).

The moving-mean value of D ln λ/Dt, calculated with (9) and (29) for a variable T, is shown in Figure 8 for cases A and C in Table 1. Good mixing occurs when the moving mean is positive, according to the criterion defined by *Ottino* [1990]. This is seen to occur, as expected, during the early phase of flow, when $t <$ 100 days, and sporadically thereafter. Spatial variability in $K(z)$ (Figure 2) is the principal cause of the resurgences in the value of ln $\lambda(T)/T$, which arise whenever a path line traverses a peak in $K(z)$. The time interval over which a resurgence persists is lengthened significantly in case C because of the slow decline in $q_z(t)$.

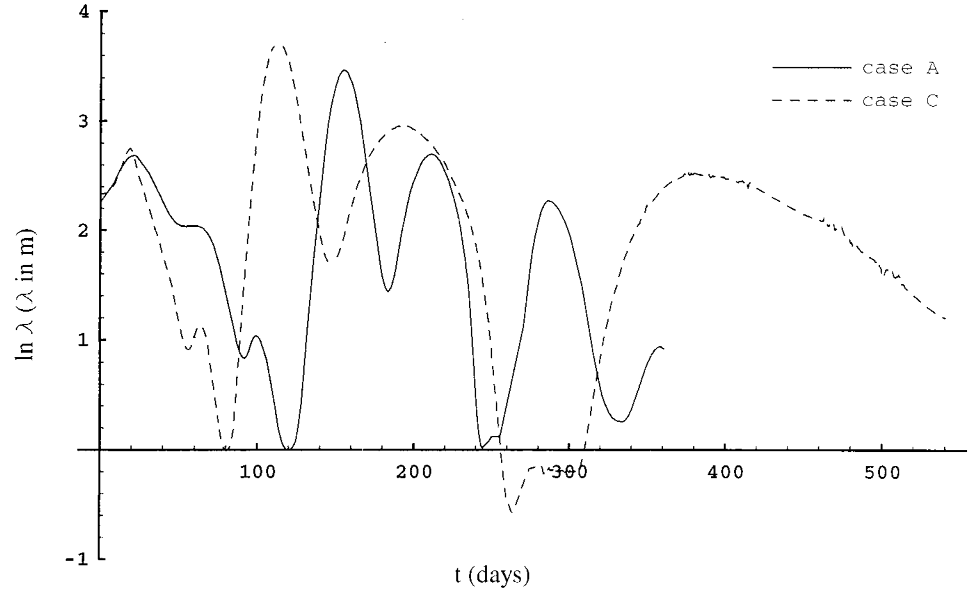

Figure 7. Natural logarithm of the length stretching λ for the three flow cases listed in Table 1, as a function of time following a path line.

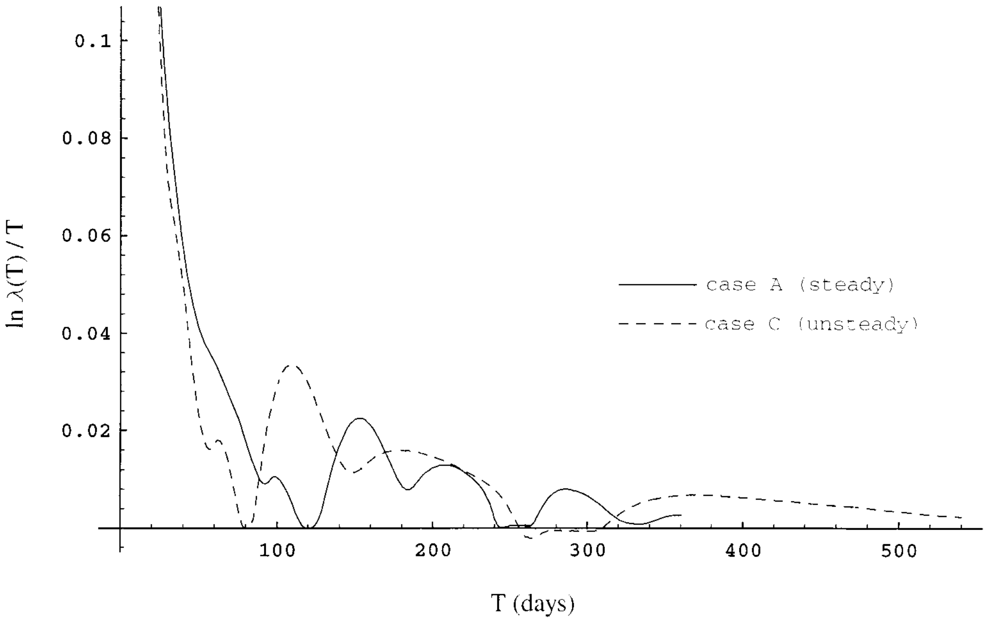

Figure 8. Temporal behavior of the moving-mean value of $\ln \lambda$ for the three flow cases listed in Table 1. The infinite-time value of this parameter is the Liapunov exponent for chaotic fluid stretching given in (10).

Ottino [1989, chapter 4] has pointed out the importance of periodic reorientation of material lines as a mechanism for increasing the efficiency of fluid mixing. This effect is seen implicitly in Figure 5, where large increases in e_λ, up to its theoretical maximum value, accompany significant changes in the direction of a path line as it traverses the boundaries between zones of highly contrasting hydraulic conductivity (compare Figures 1 and 2). However, these resurgences in e_λ do not correspond to an overall exponential time dependence of the length stretch λ, with the result that $\ln \lambda(T)/T$ gradually decays to zero (Figure 8), even under unsteady flow. This decline is in fact expected in any flow for which a stream function exists [*Ottino*, 1989, section 4.7]. In the present study, the solenoidal property of $\mathbf{q}(z, t)$ ensures the existence of a stream function [*Batchelor*, 1992, section 2.2]. Correspondingly, the Liapunov exponent in (10) must equal zero, and "Lagrangian chaos" cannot occur. Therefore the mixing of a solute plume by unsteady groundwater flow in a perfectly stratified aquifer, although definitely enhanced by pronounced spatial variability in the hydraulic conductivity and by a decreasing time dependence in the vertical component of the groundwater velocity, will not be maximally effective unless additional physical conditions are imposed to induce chaotic path lines.

Acknowledgments. The research reported in this paper was supported in part by NSF grant EAR 97-04630. Thanks to Angela Zabel for excellent preparation of the typescript.

References

Batchelor, G. K., The effect of homogeneous turbulence on material lines and surfaces, *Proc. R. Soc. London*, *Ser. A*, *213*, 349–366, 1952.

Batchelor, G. K., *An Introduction to Fluid Dynamics*, Cambridge Univ. Press, New York, 1992.

Eringen, A. C., *Mechanics of Continua*, Robert E. Krieger, Huntington, N. Y., 1980.

Farrell, D. A., A. D. Woodbury, E. A. Sudicky, and M. O. Rivett, Stochastic and deterministic analysis of dispersion in unsteady flow at the Borden tracer-test site, Ontario, Canada, *J. Contam. Hydrol.*, *15*, 159–185, 1994.

Freyberg, D. L., A natural gradient experiment on solute transportation in a sand aquifer, 2, Spatial moments and the advection and dispersion of nonreactive tracers, *Water Resour. Res.*, *22*, 2031–2046, 1986.

Kapoor, V., and P. K. Kitanidis, Concentration fluctuations and dilution in aquifers, *Water Resour. Res.*, *34*, 1181–1193, 1998a.

Kapoor, V., and P. Kitanidis, Dilution of non-reactive solutes in heterogeneous porous media, in *Scale Dependence and Scale Invariance in Hydrology*, edited by G. Sposito, chap. 10, Cambridge Univ. Press, New York, 1998b.

Kitanidis, P. K., The concept of the dilution index, *Water Resour. Res.*, *30*, 2011–2026, 1994.

Moffatt, H. K., Transport effects associated with turbulence, with particular attention to the influence of helicity, *Rep. Prog. Phys.*, *46*, 621–664, 1983.

Ottino, J. M., *The Kinematics of Mixing: Stretching, Chaos, and Transport*, Cambridge Univ. Press, New York, 1989.

Ottino, J. M., Mixing, chaotic advection, and turbulence, *Annu. Rev. Fluid Mech.*, *22*, 207–253, 1990.

Ottino, J. M., Unity and diversity in mixing: Stretching, diffusion, breakup, and aggregation in chaotic flows, *Phys. Fluids A*, *3*, 1417–1430, 1991.

Press, W. H., S. A. Teukolsky, W. T. Vetterling, and B. P. Flannery, *Numerical Recipes in C*, Cambridge Univ. Press, New York, 1992.

Roberts, P. V., and D. M. Mackay (Eds), A natural gradient experiment on solute transport in a sand aquifer. *Tech. Rep. 292*, Dep. Civil Eng., Stanford Univ., Stanford, Calif., 1986.

Sposito, G., and S. W. Weeks, Tracer advection by steady groundwater flow in a stratified aquifer, *Water Resour. Res.*, *34*, 1051–1059, 1998.

Sudicky, E. A., A natural-gradient experiment on solute transport in a sand aquifer: Spatial variability of hydraulic conductivity and its role in the dispersion process, *Water Resour. Res.*, *22*, 2069–2082, 1986.

Thierrin, J., and P. K. Kitanidis, Solute dilution at the Borden and Cape Cod groundwater tracer tests, *Water Resour. Res.*, *30*, 2883–2890, 1994.

Turcke, M. A., and B. H. Kueper, Geostatistical analysis of the Borden aquifer hydraulic conductivity field, *J. Hydrol.*, *178*, 223–240, 1996.

G. Sposito and S. W. Weeks, Department of Civil and Environmental Engineering, Hilgard Hall 3110, University of California, Berkeley, CA 94720-1710. (sweeks@nature.berkeley.edu)

(Received January 14, 1998; revised July 29, 1998;
accepted July 31, 1998.)